Equilibrium entrainment of fine sediment over a coarse immobile bed

Paul E. Grams[1,2] and Peter R. Wilcock[1]

Received 25 April 2006; revised 28 June 2007; accepted 10 July 2007; published 17 October 2007.

[1] The transported load in most fluvial systems, including gravel-bedded rivers, includes fine-grained sediment. Models for suspended sediment transport have focused on sand-covered beds, rendering incomplete the theoretical and empirical framework for predicting fine sediment transport and routing. We conducted laboratory experiments involving sand transport over large immobile grains. The experiments were scaled such that immobile particles were much larger than the mobile sediment, but less than 10% of flow depth, and that bed shear stresses, scaled by the size of the mobile sediment, were indicative of transport in suspension. The experiments were conducted in equilibrium transport and included measurements of near-bed sediment concentration and interstitial sand storage for a range of flow and transport rates. Partial filling of grain interstices occurred over a narrow range of flow and transport rates, indicating a sharp threshold between no interstitial sand storage and a sand-covered bed. Less sand coverage on the bed resulted in higher near-bed sand concentrations per unit area of sand than runs with greater sand coverage. As sand bed elevation decreased relative to the coarse grains, turbulent wakes shed by the large grains appeared to enhance grain entrainment more than the corresponding decrease in bed area covered by sand resulted in decreased entrainment. Elevated concentrations were maintained until the bed was depleted of fine sediment. These results are formalized in a proposed sand elevation correction function that scales the entrainment rate for a bed partially covered by sand to the entrainment rate that would be predicted for a sand-covered bed.

Citation: Grams, P. E., and P. R. Wilcock (2007), Equilibrium entrainment of fine sediment over a coarse immobile bed, *Water Resour. Res.*, *43*, W10420, doi:10.1029/2006WR005129.

1. Introduction

[2] The movement of fine-grained sediment through river systems is an essential component in a wide range of geomorphic, engineering, and resource management applications. For example, fine sediment transport and routing is applied in studies of watershed sedimentation [e.g., *Trimble*, 1997], fisheries management [e.g., *Lisle and Lewis*, 1992], and drainage basin evolution [e.g., *Willgoose et al.*, 1990]. Large fine sediment loads are not limited to alluvial rivers with sandy beds. In many gravel- and cobble-bedded rivers, much of the sediment load may consist of sand or finer material that is transported primarily in suspension. Indeed, fine-grained sediment comprises a significant component of the total transported load in most fluvial systems around the world [*Meade et al.*, 1990]. There is therefore a need for transport models that can be used to route fine-grained sediment over coarse substrate that remains essentially immobile during extended periods of suspended sediment transport. Existing models for fine sediment transport were developed for conditions in which the bed is uniformly composed of the same material that is in transport. When the bed sediment and the transported load are exclusively fine grained, bed forms typically develop [*Middleton and Southard*, 1984]; and their effect on the flow and transport field are considered in many models for sand entrainment [e.g., *Engelund and Hansen*, 1967; *Smith and McLean*, 1977; *McLean et al.*, 1999]. However, the dynamics of particle entrainment from a coarse bed that is only partially covered by fine sediment are poorly understood and no modeling framework addresses this situation explicitly. The purposes of this paper are to describe laboratory experiments that were conducted to investigate fine sediment entrainment over a coarse bed and to propose an entrainment relation developed from those experiments.

2. Theoretical Background

2.1. Entrainment From a Sandy Bed

[3] For the purposes of this paper, we define fine sediment as the fraction of the bed material that is typically entrained and transported in suspension, consisting of grains in the sand size range of 0.06 to 2.00 mm in diameter. Although some of the material in this size range may be transported as bed load, the majority of the flux occurs in suspension. We also refer to particles in this size range as the mobile sediment, in contrast to the coarser grains that

[1]Department of Geography and Environmental Engineering, Johns Hopkins University, Baltimore, Maryland, USA.
[2]Now at Department of Watershed Sciences, Utah State University, Logan, Utah, USA.

0043-1397/07/2006WR005129

are largely immobile for the flows that we consider. The entrainment of sediment into suspension is a function of the fluid forces acting on the sediment and the sediment characteristics. A general functional relation for sediment entrainment based on dimensional analysis was presented by *Parker and Anderson* [1977] and expanded by *Garcia and Parker* [1991]:

$$E_s = f\left(\frac{u_{*sk}}{w_s}, \frac{h}{D_{50}}, R_p\right), \tag{1}$$

where E_s is a dimensionless sediment entrainment rate, u_{*sk} is the skin friction shear velocity near the bed, w_s is the particle settling velocity, h is the flow depth, D_{50} is the median particle size for the sediment mixture, and R_p is the grain Reynolds number,

$$R_p = \frac{\sqrt{g(s-1)D_{50}}D_{50}}{\nu}, \tag{2}$$

where g is the acceleration due to gravity, $(s - 1)$ is the submerged specific gravity of sediment, and ν is kinematic viscosity. Relations for sand entrainment are founded on the theoretical equivalence of E_s with near-bed concentrations of suspended sediment for equilibrium transport conditions. This equivalence is shown by examination of the vertical fluxes of sediment in an equilibrium suspension.

[4] The instantaneous upward flux of sediment through any horizontal surface F_z is the product of the vertical velocity of the sediment W and the instantaneous concentration of suspended sediment c,

$$F_z = Wc. \tag{3}$$

[5] We assume that W can be described as the difference between a constant settling velocity w_s, which is a function of particle geometric properties and local sediment concentration, and the instantaneous vertical fluid velocity w:

$$W = w - w_s. \tag{4}$$

[6] The fluid velocity and the sediment concentration may be divided into their time average and fluctuating components yielding an equation for time average flux,

$$\bar{F}_z = \bar{w}\bar{c} + \overline{w'c'} - w_s\bar{c}, \tag{5}$$

where the overbars represent time average quantities and the primes denote the instantaneous deviations from that average (i.e., $w' = w - \overline{w}$). If the bed is nearly horizontal, it can be assumed that the time average vertical velocity is nearly zero and the time-averaged flux at some elevation a near the bed becomes

$$\bar{F}_{za} = \overline{w'c'_a} - w_s\bar{c}_a. \tag{6}$$

[7] The first term on the right-hand side in equation (6) represents the upward flux of sediment due to turbulence and the second term represents the gravitational settling of sediment. Extracting the settling velocity from those terms and defining the dimensionless rate of entrainment as

$$E_s = \frac{\overline{w'c'}}{w_s}, \tag{7}$$

equation (6) can be rewritten

$$\bar{F}_{za} = w_s(E_s - \bar{c}_a). \tag{8}$$

[8] When the bed is at equilibrium and there is no deposition or erosion of sediment, there is no vertical flux of sediment and thus the near-bed concentration equals the dimensionless rate of entrainment,

$$E_s = \bar{c}_a. \tag{9}$$

[9] *Garcia and Parker* [1991] used field and laboratory data in which near-bed sediment concentrations had been measured under equilibrium transport to evaluate the functional relation of equation (1). On the basis of these data, they proposed an entrainment relation of the form

$$E_s = \frac{AZ_m^5}{1 + \frac{A}{0.3}Z_m^5}. \tag{10}$$

[10] Z_m is a similarity variable,

$$Z_m = \frac{u_{*sk}}{w_s}R_p^n, \tag{11}$$

where $A = 1.3 \times 10^{-7}$ is a constant coefficient chosen to minimize the variation between predicted and observed entrainment rates in the data analyzed by *Garcia and Parker* [1991], and the exponent n was chosen to minimize scatter in the observed data. *Garcia and Parker* [1991] reported $n = 0.6$. The similarity variable does not include the relative roughness h/D_{50}, which *Garcia and Parker* [1991] concluded was of secondary importance to flow strength and grain size in controlling entrainment rates. The data they analyzed, however, spanned only a limited range of h/D_{50}; thus the full range of possible effects of this parameter on entrainment is incompletely understood [*Wright and Parker*, 2004]. While a formulation for fine sediment entrainment from a coarse immobile bed should share basic characteristics with this relation, there are several reasons why it may perform poorly or require substantial modifications.

2.2. Entrainment From an Immobile Coarse Bed

[11] We propose that the functional relation described in equation (1) can be expanded for sand transport over a coarse, immobile bed by including a parameter for the relative elevation of the sand bed, such that

$$E_s = f\left(\frac{u_{*sk}}{w_s}, \frac{h}{D_{50}}, R_p, \frac{z_s}{r_b}\right), \tag{12}$$

in which the additional parameter is the ratio of the sand cover thickness z_s to a characteristic roughness height for the coarse grains on the bed r_b.

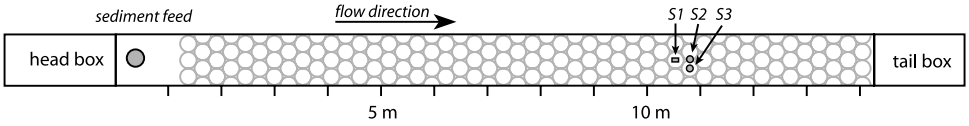

Figure 1. Sketch of the 14-m "tilting-bed" flume at St. Anthony Falls Laboratory showing configuration of the 10-cm diameter hemispheres installed as roughness elements. S1 is the suspended-sediment sampling station and ADV measurement location. S2 and S3 are additional ADV measurement locations. Streamwise distances are shown. The channel width is 0.3 m.

[12] The relative sand elevation can be argued to have either a positive or a negative effect on sand entrainment. One line of reasoning argues that the entrainment rate should decrease in proportion to the area of the bed covered by sand. As the sand bed elevation drops and the proportion of the bed area covered by sand decreases, less sand is available for entrainment resulting in lower near-bed concentrations and lower total transport rates. This effect is analogous to the findings of *Einstein and Chien* [1953], who concluded that transport for a given grain size occurs in proportion to its abundance on the bed. This effect is included in a mixed size version of the *Garcia and Parker* [1991] entrainment model provided the parameter for the proportion of sediment in each size fraction is understood to include all sediment on the bed, including immobile grains. By extension, one could infer that transport of the sand fraction of a coarse bed might occur in proportion to the abundance of sand among the bed roughness elements.

[13] Sand entrainment may, however, also depend on the elevation of the sand bed relative to the elevation of the immobile grains. The large grains may exert a hiding effect whereby sand is hidden in interstitial spaces, causing reduced entrainment. This effect has been recognized for mixed size sediments in which the presence of grains of a given size alter the mobility of grains of differing sizes [*Garcia and Parker*, 1991]. This effect could dampen entrainment rates below those predicted when the effects of the large particles are ignored.

[14] Alternatively, turbulent wakes shed by large roughness elements may enhance local scour causing evacuation of fine sediment when flow separation occurs over the coarse immobile grains. Enhanced entrainment was observed in wind tunnel experiments of a deflating sand bed with emergent large roughness elements [*Nickling and McKenna Neuman*, 1995]. They reported that transport rates increased as roughness elements initially became exposed in the deflating surface. As the sand bed elevation continued to decrease, they reported a rapid transition from enhanced transport to extremely low transport rates. They argued that the elevated transport rates resulted from increased turbulence introduced by the emerging surface roughness and that the transition to low transport rates occurred when all of the bed stress was consumed by form drag on the bed roughness elements. They observed this process to for three different roughness spacing distances and stated that the transition from enhanced transport to low transport occurred more rapidly with closer roughness spacing. A similar effect may also be inferred from the recent experiments of *Sambrook Smith and Nicholas* [2005] who investigated the different hydraulic characteristics associated with varying degrees of sand filling the spaces among gravel particles. Using an entirely immobile bed to enable flow visualization, they identified an increase in near-bed velocity and decrease in near-bed shear stress associated with an increase in the elevation of sand occupying the spaces between coarse grains. While their primary interpretation was that this indicated a decrease in the mobility of gravel relative to sand, these results may also be interpreted to suggest a decrease in the absolute mobility of all grain sizes.

3. Experimental Design and Methods

3.1. Experimental Facilities

[15] The primary objective of the laboratory experiments described in this paper was to measure near-bed sand concentration and thereby estimate the sand entrainment rate for different conditions of bed sand coverage over an immobile rough bed. The essential scaling properties for these objectives are those pertaining to the near-bed flow and sediment entrainment conditions. Thus the critical components of the experimental design are (1) a large ratio between the size of sand in transport and the size of the immobile bed material, (2) suspended sediment concentrations similar to those that occur in natural conditions, and (3) values of the Rouse number Ro less than unity indicating that the dominant mode of transport is in suspension. The Rouse number is the ratio of the particle settling velocity to the near-bed shear velocity u_*,

$$Ro = \frac{w_s}{k u_*}, \tag{13}$$

where k is von Karman's constant = 0.4. A further requirement for these experiments was near-equilibrium transport conditions such that measured values of $\bar{c}_a$ can be used to estimate E_s (equation (9)).

[16] The experiments were conducted in a 14-m-long flume with a working width of 0.3 m at the St Anthony Falls Laboratory (Figure 1). Bed roughness was created by attaching 10-cm diameter hemispheres to the flume bed in a closest-packing arrangement. Although the immobile component of the bed in natural settings can be orders of magnitude larger, the ratio between this size and the fine component is large (>800) and should ensure that essential interactions between the two bed grain size components are represented. The packing arrangement was chosen to represent the effect of a bed of well-sorted cobbles in a natural channel. Although different packing arrangements may be used to represent other bed configurations, we believe that the closest packing arrangement is the most general case and that the effects of other immobile grain configurations are likely to be secondary. The goal of this design was to isolate the interaction between the mobile fine sediment and the immobile coarse grains.

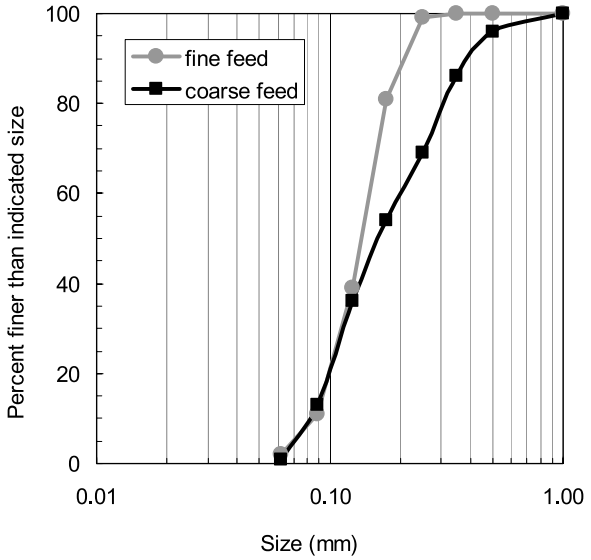

Figure 2. Grain size distribution of feed sediments.

[17] Two sediment mixtures were used for the fine-sediment feed. The "fine" sediment was natural grain quartz sand with a median diameter of approximately 0.13 mm (US Silica F110); the "coarse" sediment was a natural grain sand mixture with a median diameter of approximately 0.17 mm (Figure 2). These sizes are within the range of sand grain sizes that comprise the fine fraction of the bed material load of many rivers.

[18] The bed slope was set at 0.0002 with a flow depth of 40 cm (measured from the top of the hemispheres to the water surface) such that *Ro* was between about 0.5 and 0.7. This range of *Ro* is representative of conditions for which the majority of bed material transport occurs in suspension. A 40-cm flow depth was chosen such that the flow would include both a spatially variable near-bed region and a spatially integrated region away from the bed. The resulting ratio of flow depth to grain size is roughly an order of magnitude smaller than occurs in the field. This distortion is likely to affect the frequency and magnitude of the largest turbulent eddies that reach the near-bed region. The effect of those processes on sand entrainment should be secondary to the effects of flow separation and wake turbulence within the near bed region caused by the roughness elements. Measurements of velocity profiles indicated that the flow depth was sufficient to produce both a near-bed spatially variable layer and a thicker spatially averaged layer in the core of the flow.

[19] Sediment was fed into the upstream end of the flume through a pipe that introduced the sediment near the bed to ensure rapid mixing. Constant sediment feed rates were maintained by an automated sediment feeder or by adding sediment from containers of known volume at timed intervals. Sediment concentrations were between 500 and 2500 mg/l. Water surface elevations were measured to monitor flow conditions.

[20] For each sediment feed rate, a series of experimental runs was conducted using different flow rates to establish conditions producing a uniform sediment bed and transport field (Table 1). Flume discharge Q was measured directly in large volumetric tanks and used to calculate mean velocity

$$U = Q/bh, \tag{14}$$

where b is the flume width and h is the measured flow depth. Each run was started with no sand on the bed and run durations were determined such that the total volume of sand feed exceeded the maximum available bed storage by a factor of three or greater. For the final 2 to 5 minutes of most runs, the sand feed was replaced with a colored sand feed of the same size in order to allow observations of sediment mixing within the bed.

3.2. Data Collection

[21] Samples of suspended sediment were collected at one sampling location 10.5 m downstream from the flume head box (Figure 1). This location was chosen because it was well downstream from entry effects caused by flow exiting the head box and the beginning of the rough bed at the head of the flume. Samples were drawn from the flow by a rake of stainless steel 3.18 mm internal diameter Pitot tubes with nozzles positioned at elevations of 0.5, 2, 5, 10,

Table 1. Flume Run Characteristics and Final Bed Condition

Run	Q[1], l/s	Q_s[1], g/s	U[1], m/s	Run Time, hours	Fr[1]	R_o[1]	Feed	$\bar{z}_s$,[a] cm	Bed Condition
0	98	75	0.81	2.2	0.40	0.36	fine	0	no sand cover
6a	97	200	0.80	0.8	0.40	0.37	fine	0	no sand cover
3	66	75	0.56	2.0	0.28	0.52	fine	0.9	minimal sand cover
14	66	41	0.55	2.5	0.28	0.53	fine	1.0	minimal sand cover
2	71	75	0.59	2.0	0.30	0.49	fine	1.0	minimal sand cover
13	71	43	0.59	2.2	0.30	0.49	coarse	1.6	partial sand cover
15	66	20	0.55	2.0	0.28	0.53	coarse	1.9	partial sand cover
16	79	46	0.66	3.0	0.33	0.44	coarse	2.2	partial sand cover
17	93	179	0.78	1.3	0.39	0.38	coarse	2.9	partial sand cover
6b	92	200	0.76	1.1	0.38	0.39	fine	1.2	partial sand cover
8	60	33	0.50	2.5	0.26	0.58	fine	1.9	partial sand cover
12	60	75	0.50	1.3	0.25	0.58	fine	3.1	partial sand cover
7	53	33	0.45	2.5	0.23	0.64	fine	2.0	aggrading-small dunes
5	88	200	0.73	1.0	0.36	0.40	fine	2.0	aggrading-small dunes
1	53	75	0.45	2.1	0.23	0.64	fine	8.1	aggrading-large dunes
4	79	200	0.67	1.3	0.34	0.44	fine	9.4	aggrading-large dunes

[a] Q is discharge, Q_s is sediment feed rate, U is mean velocity, Fr is Froude number, Ro is Rouse number, and $\bar{z}_s$ is the mean elevation of sand in the bed at the conclusion of the run.

and 30 cm above the hemisphere tops. Each Pitot tube was attached to a length of plastic tubing that carried the sample to a collection jar. Prior to sampling the suspended sediment, point velocities at each sampling location were measured with an acoustic Doppler velocimeter (ADV; SonTek 10-MHz). Velocity through the sampling tube was adjusted to match that of the local flow by adjusting the elevation of the siphon tube outlet. Between one and five sets of suspended sediment samples were collected for each run and sample durations ranged from 30 to 60 s. A total of 294 suspended sediment samples were collected and analyzed to determine sand concentration [*Grams*, 2006]. A subset of these samples, including the final sample for each run, was processed in a settling tube to determine the grain size distribution.

[22] For each of the flow rates used in the experimental runs, a set of velocity profiles were measured with the ADV. All velocity measurements were made prior to experimental runs when there was no sand on the bed or in suspension. There was insufficient time during the experimental runs to collect velocity profiles under conditions of partial sand cover on the bed. Velocity profiles were measured directly over a hemisphere in the center of the channel at the sediment sampling location and on the right side of the channel one row downstream from the sampling location. A third profile was collected over the gap between two spheres one row downstream from the sediment sampling location (Figure 1). Each profile consisted of seven velocity measurements made 0.5, 1, 2, 5, 10, 20, and 30 cm above the height of the hemisphere tops. Individual velocity measurements were collected at a 25 Hz sampling rate for a period of one minute. The ADV measured velocities in three orthogonal coordinates within a 0.2 cm^3 sample volume.

[23] The raw ADV data were processed to remove spikes. Spikes in ADV data are caused by aliasing of the Doppler signal that can occur when the velocity exceeds the set velocity range or as a result of signal contamination from previous pulses reflected from complex bottom geometries. Because measured velocities never approached the limit of the sampling range (2.50 m/s), all of the spikes in the ADV records are likely due to the bottom geometry. These spikes were removed by a phase space threshold despiking method described by *Goring and Nikora* [2002] and implemented in the WinADV software by *Wahl* [2000, 2003]. *Goring and Nikora* [2002] found this method the most satisfactory in detecting anomalous spikes while leaving intact true spikes due to turbulent fluctuations in the velocity. Spikes detected by this method were removed from the record. Mean velocities and turbulence statistics were calculated from the filtered data. The turbulent Reynolds stress associated with the plane parallel to the bed τ_{zx} was calculated at each elevation in the flow as

$$\tau_{zx}(z) = -\rho\overline{(u'w')}, \tag{15}$$

where z represents height above the bed, ρ is the fluid density, u and w are the instantaneous streamwise and vertical components of velocity, taken positive in the downstream and upward directions, the overbars represent time-averaged quantities and the primes denote instantaneous deviations from the mean. The corresponding shear velocity was calculated as

$$u_*(z) = \sqrt{\tau_{zx}(z)/\rho}. \tag{16}$$

[24] We define the shear velocity here as a profile because when nondimensionalized by the mean velocity it provides an effective comparison of the measured Reynolds stresses among the runs conducted at different mean velocity. Thus $u_*(z)$ is used to denote the shear velocity at height z above the bed, while u_* is the shear velocity at the boundary according to the conventional definition (i.e., $u_* = \sqrt{\tau_0/\rho}$), where τ_0 is the boundary shear stress.

[25] Following each run, the entire length of the hemisphere-covered bed was photographed from above in 0.5 m sections. The depth of sand was measured directly along the centerline and along each sidewall every 20 cm. All measurements were made in the interstices from a common bed reference elevation at the base of the hemispheres. This would correspond to the average low-point elevation of interstitial spaces in a bed of natural grains. The measured depths were averaged to calculate the mean sand cover thickness $\bar{z}_s$ for the channel. The depth of colored sand mixing was determined by measuring the depth of colored sand occurrence at each of these locations for runs in which colored sand was used. Bed samples were collected at approximately 2-m intervals along the flume bed. Separate surface and subsurface samples were collected where there was a difference in surface and subsurface grain size or sediment color.

3.3. Flow Structure and Characterization of Bed Stress

[26] Because bed slope and the average depth were the same for each of the experimental runs, most of the hydraulic adjustment over the 50% variation in discharge occurred in the mean velocity (Table 1). This resulted in slightly nonuniform flow conditions at the flume entrance and exit. During the experimental runs, depths at the upstream and downstream ends of the flume were measurably different than the depths in the center region, which extends from 4 to 12 m downstream from the head box. At 2 m downstream from the head box, depths were up to 1.3 cm greater than the average depth in the center region $\bar{h}$ and at 13.6 m downstream, depths were up to 1.4 cm greater than the average depth in the center region. Depths in the center region were all within 0.4 cm, (1.0 percent) of the average depth (Figure 3).

[27] The velocity profiles collected in the vicinity of the sediment sampling station indicate that the flow was well mixed vertically in the first 2 cm above the hemispheres (Figure 4). From 0.5 to 2 cm above the hemispheres, velocities are constant within the range of uncertainty in the measurements. Between 2 cm and 30 cm above the roughness elements, velocity increases in a log linear relationship. The mean velocity occurs between $0.25z/h$ and $0.5z/h$. Similar velocity profiles, characterized by separate near-bed and outer regions, have been previously reported over very rough beds [*Nowell and Church*, 1979; *Byrd et al.*, 2000].

[28] We used the turbulent velocity profiles to calculate bed stress for each of the flow rates. The mean $u_*(z)/U$ from 0.5 to 2 cm above the hemispheres is similar among the

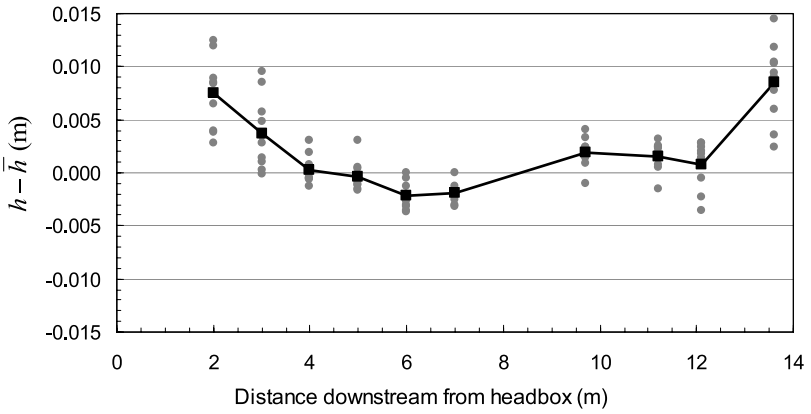

Figure 3. Deviation in flow depth for all experimental runs with minimal or partial sand cover. The gray circles are the deviation in depth for each run, and the black squares and solid line show the average. The deviation in flow depth is the difference between the measured depth at each location h and the mean flow depth in the center region (4–12 m) $\bar{h}$.

three different measurement stations, and the variation is not correlated with the magnitude of the mean flow velocity (Figure 5). This pattern suggests that for these experimental conditions, stress near the bed can be approximated as a simple function of mean velocity

$$u_* = 0.07U. \tag{17}$$

[29] Analysis of the residuals of u_* calculated from equation (17) compared to the measured values of $u_*(z)$ at 0.5, 1.0 and 2.0 cm indicate a root-mean-square error of 0.01. The error is approximately the same among the different measurement positions and elevations.

[30] We compared the estimate of stress based on equation (17) with an estimate based on the shallow water equation

$$\tau_{0,SW} = \rho g R\left[S_0 - \frac{dh}{dx} - \frac{U}{g}\frac{dU}{dx}\right], \tag{18}$$

where $\tau_{0,SW}$ is the total boundary shear stress, S_0 is the slope of the flume bed, and R is the hydraulic radius given by $R = bh/(b + 2h)$. The gradients in depth and velocity were determined by backward differences from each measurement position, starting with the second station downstream. The shallow water equation yields an estimate of total boundary stress, whereas equation (17) based on the Reynolds stress is an estimate of bed stress. The difference between these measures of stress results from stress on the flume sidewalls. To compare these, we applied the flume sidewall correction procedure of *Vanoni* [1975] (modified by *Chiew and Parker* [1994]) to the bed stress calculated from equation (17) to estimate total boundary shear stress $\tau_{0,RS}$. In the sidewall correction, the bed friction factor is calculated on the basis of the friction factor for the total flow and for the hydraulically smooth sidewall. The sidewall friction factor is estimated from a standard relation between friction factor and Reynolds number **Re** for a hydraulically smooth surface:

$$\mathbf{Re} = 4UR/\nu. \tag{19}$$

[31] The bed portion of the shear stress $\tau_{b,RS}$ is then calculated from the bed friction factor. The total stress $\tau_{0,RS}$ is related to $\tau_{b,RS}$ and the wall stress $\tau_{w,RS}$ as

$$\tau_{0,RS}PL = \tau_{b,RS}bL + \tau_{w,RS}2hL, \tag{20}$$

where L is a length of bed in the streamwise direction and P is the wetted perimeter for a rectangular flume $P = b + 2h$. The modeled bed stress is approximately 2.5 times the wall stress and 1.8 times the total stress. Figure 6 shows $\tau_{0,SW}$

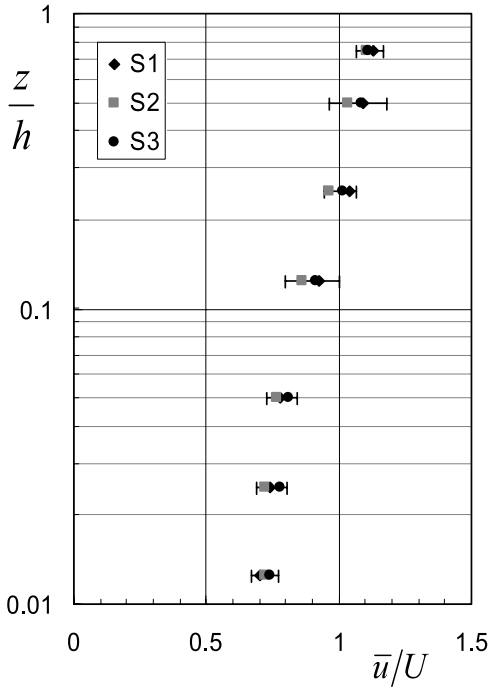

Figure 4. Profiles of normalized mean streamwise velocity for each of the three measurement stations near the sampling station. The locations of the measurement stations are indicated in Figure 1. The error bars show plus or minus one standard deviation about the mean for all measurement stations.

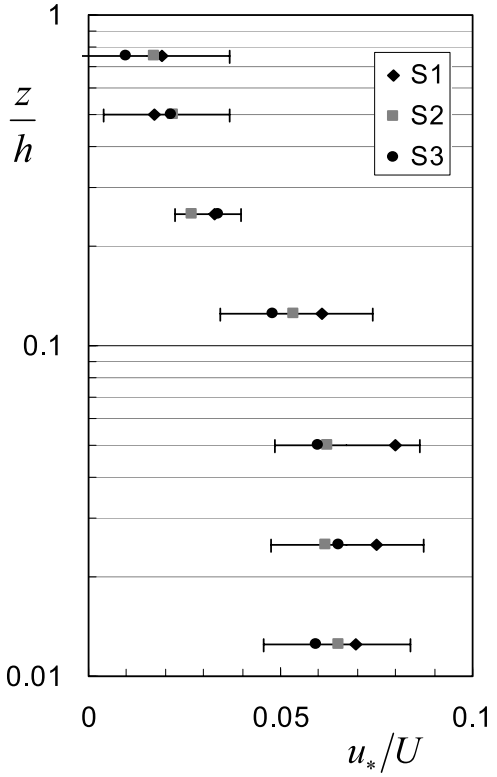

Figure 5. Profiles of normalized shear velocity for each of the three measurement stations near the sampling station. The locations of the measurement stations are indicated in Figure 1. The error bars show plus or minus one standard deviation about the mean for all measurement stations.

compared with $\tau_{0,RS}$. Although there is scatter in the boundary stress calculated from the shallow water equation, that estimate of stress is generally consistent with the bed stress calculated from equation (17). Thus the simple relation between bed stress and mean velocity (equation (17)) based on the near-bed Reynolds stress provides a convenient measure of bed stress that is also consistent with estimates based on measured parameters of the bulk flow.

3.4. Evaluation of Grain Stress

[32] Some fraction of the bed stress is grain stress that contributes to the entrainment of mobile grains while the remainder is consumed by form drag on the immobile grains and bed forms [e.g., *Engelund and Hansen*, 1967; *Smith and McLean*, 1977; *van Rijn*, 1984; *Wiberg and Smith*, 1991]. In our experiments, the sand was nonuniformly distributed among the roughness elements, such that some was near the bottom of the interstitial spaces and some was at elevations at or near the top of the roughness elements. This condition existed for all of the runs with sand cover on the bed, and there was never a situation where the sand partially filled the interstitial spaces to an even depth throughout the channel (Figure 7). Thus both the immobile grains and the configuration of the mobile sediment contribute to the form drag. The bed was never configured such that one can reasonably assume that the sand bed was subject to the same grain stress everywhere. *McLean et al.* [1999] identified essentially the same problem in the calculation of entrainment of sand into suspension from bed forms. They determined that most entrainment occurred near the top of a bed form where the grain stress was higher than in the dune troughs. Instantaneous measurements of Reynolds fluxes have also shown large spatial and temporal variations of local stress in the presence of bed forms or other large roughness elements [*Nelson et al.*, 1995; *McLean et al.*, 1999]. Thus any estimate of grain stress for a channel segment is a spatially averaged compromise and does not correspond directly to local grain stress that is causing entrainment from a particular location on the bed.

[33] We estimated the grain stress using the *Einstein and Barbarossa* [1952] method of stress decomposition, which is commonly used in the type of sand entrainment formulation on which we build [e.g., *Engelund and Hansen*, 1967; *Garcia and Parker*, 1991; *Wright and Parker*, 2004]. At the core of this approach is the analogy between the flow of interest and a hypothetical flow that has the same slope and mean velocity but lacks the drag exerted by bed forms and immobile grains. The mean velocity is related to the bed stress through a standard resistance relation

$$\frac{U}{u_*} = \frac{1}{k}\ln\left(\frac{11h}{k_s}\right), \tag{21}$$

where k_s is the Nikuradse equivalent grain roughness associated with the total bed stress. By the analogy of the Einstein decomposition, a similar relation holds for the hypothetical flow:

$$\frac{U}{u_{*sk}} = \frac{1}{k}\ln\left(\frac{11h_{sk}}{k_{s,sk}}\right), \tag{22}$$

where h_{sk} is the flow depth due to grain stress and $k_{s,sk}$ is the skin friction roughness height. Here $k_{s,sk} = 2.5D_f$ is used,

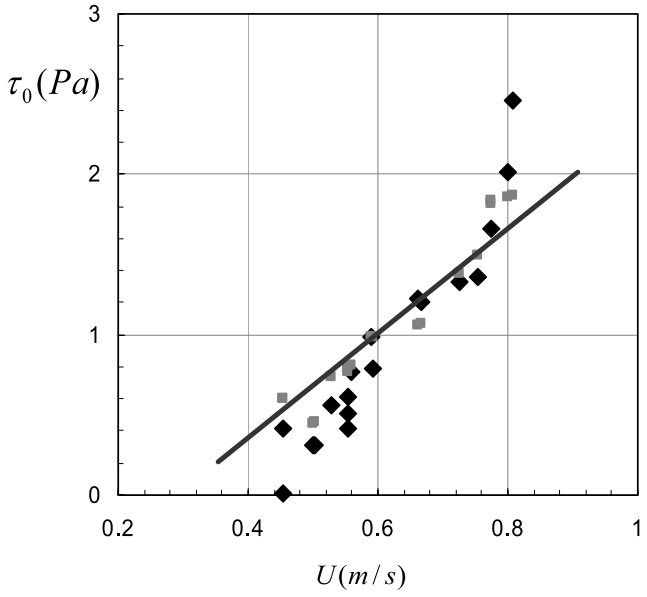

Figure 6. Comparison of total boundary shear stress estimated using the shallow water equation (black diamonds) to the total boundary shear stress calculated by applying the sidewall correction procedure to the bed stress determined from the near-bed Reynolds stresses (gray squares). The solid line shows the total stress approximated from equation (17) with the sidewall correction applied.

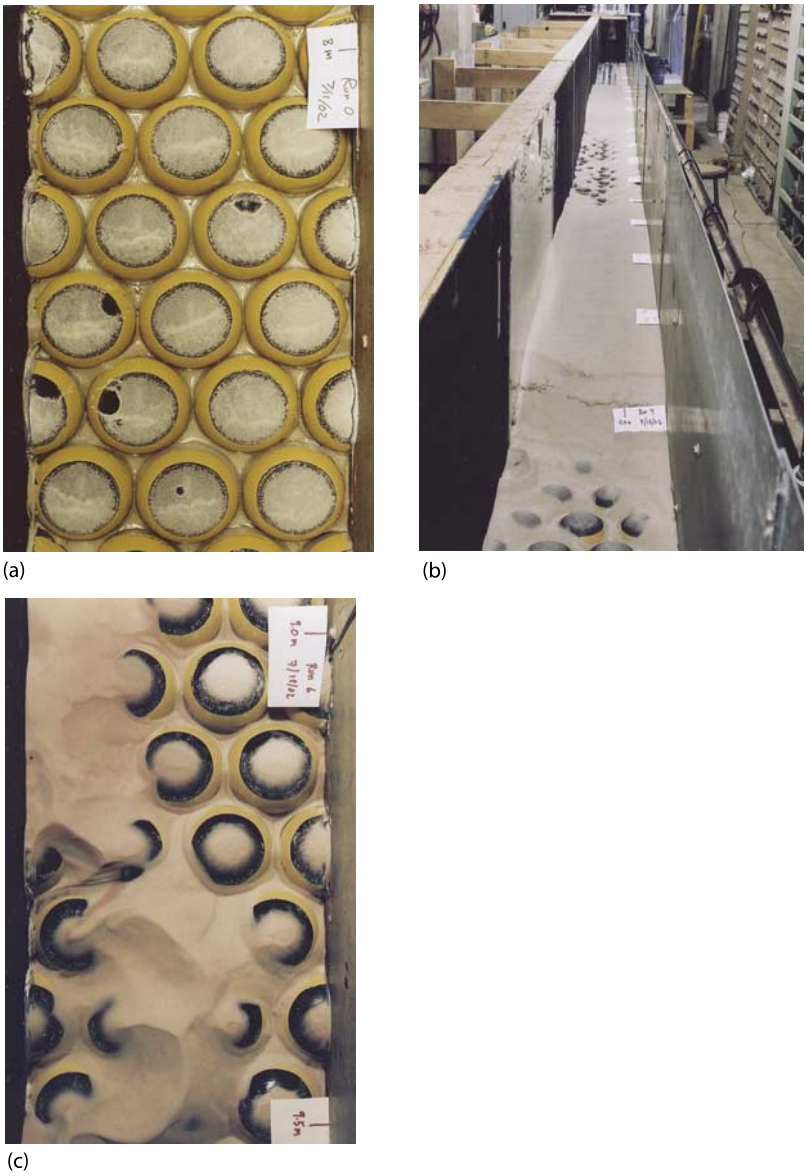

Figure 7. Photographs showing (a) postrun bed condition for an evacuated bed in run 0, (b) aggrading bed with large dunes in run 4, and (c) bed partially covered with sand in run 6b. The water discharge and sediment feed rates are listed in Table 1. The sand covering the hemisphere tops settled from suspension after flow was stopped.

where D_f is the median fall diameter of the mobile sediment. This value was used by *Engelund and Hansen* [1967], which was the method followed by *Garcia and Parker* [1991]. The energy slope S of the hypothetical flow is also the same as that of the flow in question; thus

$$u_* = \sqrt{ghS} \tag{23}$$

$$u_{*sk} = \sqrt{gh_{sk}S}. \tag{24}$$

[34] Combining equations (23) and (24),

$$\frac{u_{*sk}}{u_*} = \sqrt{\frac{h_{sk}}{h}}. \tag{25}$$

[35] Given the total stress and the mean velocity, equations (22) and (25) can be solved iteratively for the grain stress. Because we estimated u_* independently (equation (17)), equation (21) is not required and the total flow roughness k_s is not involved in this calculation.

[36] It is important to note that this method does not include an explicit calculation of form drag. Any flow with the same energy gradient and mean velocity is assumed to posses the same form drag and grain stress if the mobile particles have the same size distribution. However, in our application the local grain stress is spatially variable and the effect of this unequal distribution of grain stress is, in essence, the phenomena that we seek to investigate. Because we use a method for the calculation of grain stress that does not vary as the relative exposure of the partially buried roughness elements varies, we relegate all variability in the entrainment rates to our entrainment formulation,

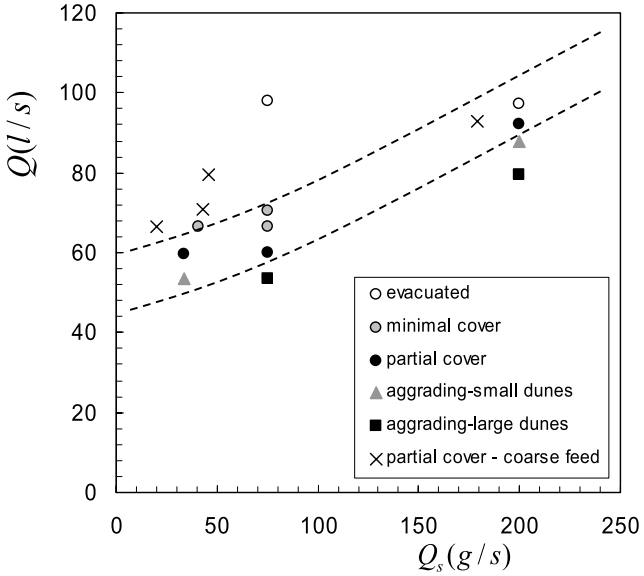

Figure 8. Plot of sediment feed rate (Q_s) and flow rate (Q) for uniform transport runs conducted in 2002. The dashed lines identify the narrow range of Q for which a given Q_s will produce a bed of partial sediment cover for the fine sediment feed, which is one with deposition of sand among the sphere interstices, but without massive aggradation that forms migrating dunes. The coarse sediment feed requires a larger discharge to create partial sand cover.

which does depend on the condition of the sand bed. Thus the Einstein stress decomposition is consistent with our approach, which is to examine the integrated effects of spatially variable grain stress and other factors related to sand bed configuration on near-bed suspended sediment concentrations.

4. Results

4.1. Observations on the Formation of a Sediment Bed

[37] For each sediment feed rate, a partially sand covered bed was developed and maintained only for a narrow range of flows. At discharges above this range, most of the sediment remained in suspension and very little or no sand bed developed. For example, in run 0 that had a discharge of 98 l/s and a sediment feed rate of 75 g/s, no sediment bed formed (Figure 7a). In run 1 where the discharge was 53 l/s and the feed rate was the same as run 0 and in run 4 with a discharge of 79 l/s and a feed rate of 200 g/s, sediment accumulated on the bed and migrated downstream as a coherent dune (Figure 7b). Within a certain range of water discharge and sediment feed, sand accumulated in the hemisphere interstices, resulting in partial sand coverage but no dune formation. This occurred in run 6b, which had a discharge of 92 l/s and a sediment feed rate of 200 g/s (Figure 7c). The partial sand bed elevation was typically reached about midway during a run and maintained for the remainder of the run. However, even in the runs for which the mean sand bed elevation was less than the height of the hemispheres, the hemispheres were sometimes buried locally (Figure 7c). The greatest sand depths were concentrated along the sidewalls, driven by reduced velocity and bed shear near the wall. Those experiments that resulted in a bed with some sediment retention but without sustained aggradation and dune formation, were divided into runs with an average sand depth of 1 cm or less (minimal sand cover) and runs with an average sand depth of greater than 1 cm (partial sand cover). The runs without a stable sand bed were classified as either "dune-forming" or "evacuating" runs, depending on whether dunes formed or no sediment bed formed, respectively. Two of the dune forming runs resulted in large dunes that covered much of the flume bed and resulted in an average sand depth that exceeded the bed roughness height. Smaller dunes formed in the other two dune-forming runs and average sand depths were less than the bed roughness height.

[38] Bed conditions with minimal or partial sand cover were achieved for six sediment feed-discharge combinations (Figure 8). For example, at the sediment feed rate of 75 g/s, there was one run in which the bed aggraded and formed large dunes. At slightly higher discharges, beds with partial and minimal sand cover were achieved. The transition from runs with an aggrading bed to runs with an evacuated bed was most narrowly defined for the runs conducted at a sediment feed rate of 200 g/s. This feed rate combined with a discharge of 92 l/s produced a partially sand covered bed. The slightly higher discharge of 97 l/s resulted in an evacuated bed and the slightly lower discharge of 88 l/s caused a small dune to form. The lower discharge of 79 l/s resulted in a large dune.

[39] These results suggest that a partially sand-covered bed may not be a stable condition and that the transition from full sand cover to a bed with low sand elevations can occur abruptly. The rapid transition from aggrading to evacuating conditions may indicate that as the sand elevation drops below the tops of the roughness elements, entrainment rates are maintained approximately at the full sand bed rate or, perhaps, elevated. If entrainment rates declined rapidly as the bed roughness elements were exposed, the condition of partial sand cover should be more stable and we would observe a wider range of discharge and feed rates that produced partial sand coverage. This interpretation is consistent with the observation by *Nickling and McKenna Neuman* [1995] of enhanced entrainment as roughness elements became exposed in aeolian transport. Because intergrain collisions are less important in accelerating entrainment in water than in air, we would expect to have a smaller degree of enhanced entrainment than observed by *Nickling and McKenna Neuman* [1995].

4.2. Vertical Distribution of Suspended Sediment and Determination of the Reference Elevation

[40] We used measured profiles of suspended sediment concentration to determine the appropriate sediment concentration reference elevation. It was shown above that for equilibrium transport, the near-bed concentration is equal to the dimensionless rate of particle entrainment. The reference elevation a is not universally agreed upon, but is usually taken to be near the bed, either scaling with the grain size of the sediment in transport [e.g., *Engelund and Fredsoe*, 1976] or flow depth [e.g., *Celik and Rodi*, 1988; *Garcia and Parker*, 1991]. Often, the selection of a reference elevation is driven by practical considerations to be the lowest elevation at which accurate measurements of suspended sediment concentration are possible. For a specified reference elevation, the vertical distribution of suspended

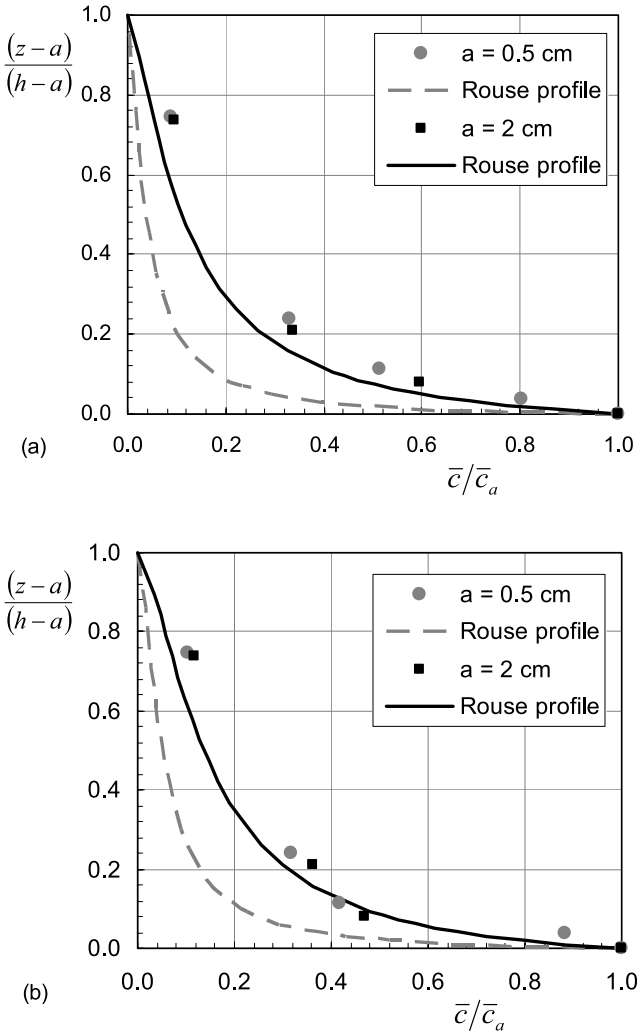

Figure 9. Measured suspended sediment concentrations normalized by the reference elevation and the near-bed concentration and modeled profiles of sediment concentration based on Rouse distribution calculated for the indicated near-bed reference elevation a. Data are from experimental runs (a) 12 and (b) 14.

sediment for an equilibrium bed and steady, uniform flow is given by the Rouse distribution [*Rouse*, 1937]

$$\frac{\bar{c}}{\bar{c}_a} = \left[\frac{(h-z)/z}{(h-a)/a}\right]^{Ro}. \tag{26}$$

[41] Measured profiles of suspended sediment concentration are shown in Figure 9 together with theoretical profiles, calculated using equation (26) and the measured concentration at the indicated reference elevation c_a. These profiles show that concentrations in the upper part of the flow are best predicted by the Rouse distribution when the reference elevation is 2 cm. This behavior is consistent with the vertical structure of the velocity profile over the bed roughness elements (Figure 4). The Rouse distribution is based on a logarithmic velocity profile, which did not exist in the lower 2 cm of the flow (Figure 4). The elevation of 2 cm is equivalent to 0.05 h, which is among the more frequently used measures of the reference elevation [*Itakura and Kishi*, 1980; *Celik and Rodi*, 1988; *Garcia and Parker*, 1991].

[42] The measured profiles of suspended sediment concentration were vertically integrated to determine the load and the average concentration of suspended sediment. For the runs with minimal or partial sand cover, the concentration of sand transported in suspension near the end of the run was similar to the concentration of sand fed at the upstream end of the channel (Figure 10). For the runs with dunes forming on the bed, the output concentration tended to be less than the feed concentration. This indicates that for the runs with minimal and partial sand cover, near-equilibrium conditions were achieved.

4.3. Near-Bed Concentrations and the Sand Elevation Correction Function

[43] The rapid transition from a bed that is fully sand covered through a state of partial sand cover to a bare bed with essentially no sand cover indicates that, for some range of average sand bed elevations between $z_s = 0$ and $z_s = r_b$, the rate of sand entrainment per unit bed area covered by sand should be greater than that which would occur from a completely sand-covered bed. To examine this possibility, we calculate entrainment for a sand-covered bed $\hat{E}_s$ as a reference condition and we compare the observed near-bed concentrations with those that would be predicted if entrainment scaled directly with the area of sand cover on the bed. Figure 11 shows entrainment predicted by the *Garcia and Parker* [1991] entrainment model (equation (10)) compared with observed near-bed concentrations $\bar{c}_{a,obs}$ and the same near-bed concentrations normalized by the proportion of bed covered by sand $\hat{c}_a$,

$$\hat{c}_a = \frac{\bar{c}_{a,obs}}{A_s}, \tag{27}$$

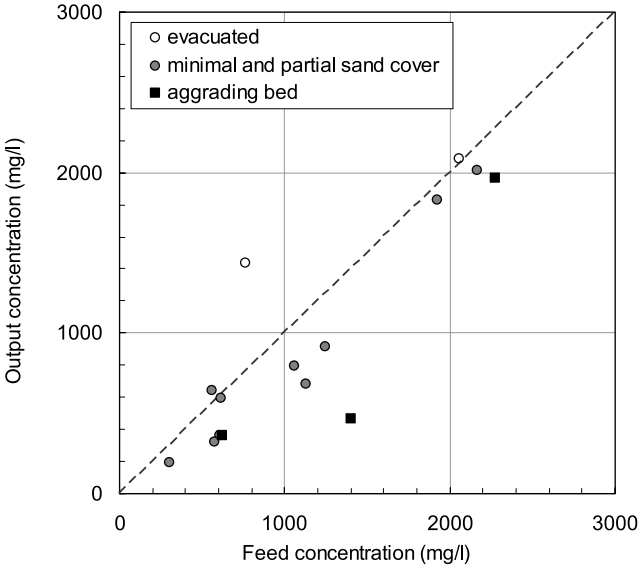

Figure 10. Comparison between measured sediment concentrations (output concentration) and the concentration of sediment fed at the upstream end of the flume (feed concentration). Similar output and feed concentration for the runs with minimal and partial sand cover indicate an equilibrium bed state.

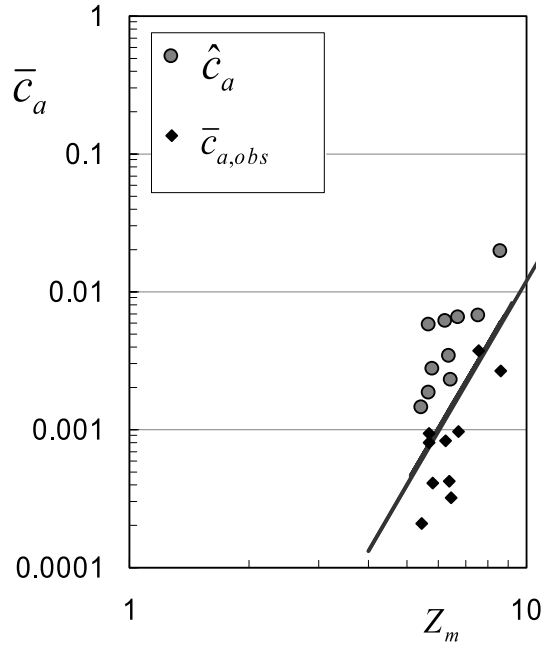

Figure 11. The near-bed sand concentration predicted by the *Garcia and Parker* [1991] entrainment model (sold line) and the observed concentrations at 2 cm above the hemisphere tops (black diamonds). The shaded circles show the observed concentrations normalized by the area of bed that was covered by sand.

where A_s is the proportion of the bed covered by sand. In calculating entrainment using equation (10), we used the grain stress determined by the Einstein decomposition (equations (22)–(25)). The near-bed concentration was evaluated at 5% of the flow depth (2 cm) and only observations from runs resulting in minimal or partial sand cover (Table 1) and equilibrium bed state were included. The observed concentrations are smaller than predicted by the entrainment model, which suggests that concentrations for conditions of partial sand cover were smaller than concentrations that would be predicted for the same flow over a full sand bed. However, the observed concentrations per unit bed area covered by sand are larger than predicted by the entrainment model. This suggests that the rate of entrainment per unit area of bed covered by sand is larger for conditions of partial sand cover than for a full sand bed.

[44] These results can be expressed in terms of a sand elevation correction function that relates the entrainment rate over a partially sand-covered bed E_s to the entrainment rate predicted by the *Garcia and Parker* [1991] entrainment model for a sand-covered bed, $\hat{E}_s$. Because the bed for these runs was at or near equilibrium, the observed near-bed concentrations $\overline{c}_{a,obs}$ are used as an estimate of the actual entrainment rate (equation (9)). The sand elevation correction ε is defined

$$\varepsilon = \frac{\overline{c}_{a,obs}}{\hat{E}_s}. \tag{28}$$

[45] Figure 12 shows ε plotted as a function of the normalized sand bed elevation $\hat{z}_s$, where

$$\hat{z}_s = \frac{\overline{z}_s}{r_b}. \tag{29}$$

[46] Although there is scatter in the plotted data, a rapid increase in the entrainment rate for $0.1 < \hat{z}_s < 0.5$ is indicated. The function shown in Figure 12 is a logistic function that was chosen to fit the observations for $\varepsilon \leq 1$. The data suggest a function that increases steeply between $\hat{z}_s = 0.1$ and $\hat{z}_s = 0.4$, but the strongest constraints are those imposed at the extremes of the function. As the bed approaches full sand coverage, the entrainment must approach that of a full sand bed, and as the sand bed elevation approaches zero the net rate of entrainment must approach zero. Thus some function that increases from zero to one is expected. Although there are two data points where $\varepsilon > 1$ and it is possible that entrainment rates could exceed those predicted for a full sand bed for a range of partial sand bed elevations, those data are few and, given the range of scatter indicated by the other data, may not be significantly different than $\varepsilon = 1$. The logistic function shown in Figure 12 is given by

$$\varepsilon_L = \left(1 + e^{-\xi\left(\hat{z}_s - Z^*\right)}\right)^{-\eta}, \tag{30}$$

with $\xi = 18$, $Z^* = 0.2$, and $\eta = 1.1$.

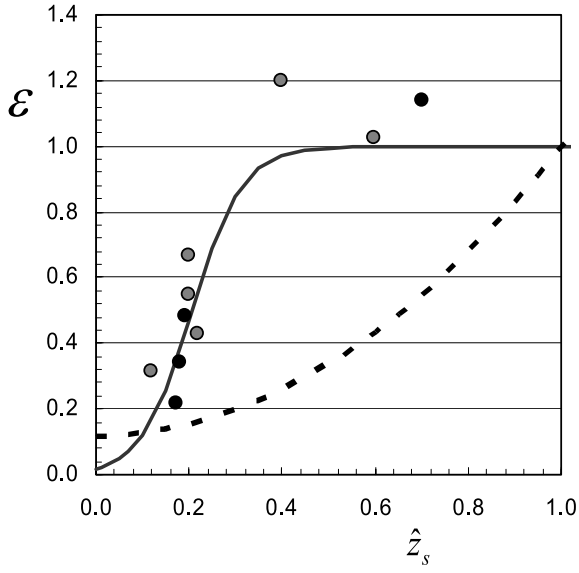

Figure 12. Sand elevation correction ε plotted as a function of the normalized sand bed elevation $\hat{z}_s$. The data points are the ratio of observed near-bed concentrations to concentrations predicted for a full sand bed (equation (28)) for the fine (gray symbols) and coarse (black symbols) feed. The solid line is the logistic function (equation (30)), and the dashed line is a function for the area of exposed sand (equation (32)). For $\varepsilon < 1$, entrainment rates are lower than would occur over a sand bed, and for $\varepsilon > 1$, entrainment rates are higher than over a sand bed.

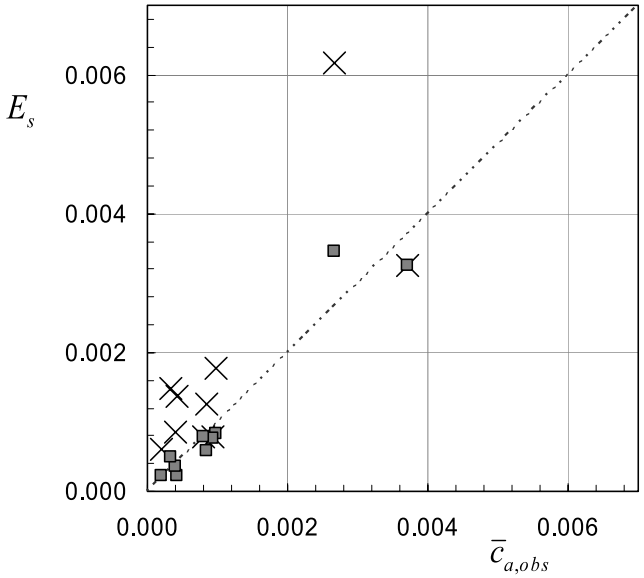

Figure 13. Comparison between measured near-bed concentration and predicted entrainment rate. Entrainment predicted using the sand elevation correction (squares) matches observed near-bed concentration better than entrainment predicted without the sand elevation correction (crosses) for most observations. The dashed line is a line of perfect agreement.

[47] The proposed rough bed entrainment correction is compared with a correction based solely on the fraction of the bed that is covered by sand:

$$\varepsilon_A = A_s. \tag{31}$$

[48] For hemispheres the area of sand is related to the sand depth by

$$A_s = \frac{b - N\pi\left(r_b^2 - \bar{z}_s^2\right)}{b}, \tag{32}$$

where N is the number of hemispheres per meter of channel length. This function predicts entrainment rates lower than were observed for most conditions of partial sand cover. Entrainment rates predicted with the logistic function (equation (30)) are compared with the measured near-bed concentrations in Figure 13. Use of the sand elevation correction reduces the scatter in the predicted concentrations and results in a better match between predicted and observed concentrations.

5. Discussion and Conclusions

[49] Prediction of the sediment entrainment rate is a critical component of any fine sediment transport and routing model. Primary controls on the entrainment rate are the grain size of the available sediment and the shear stress at the bed, both of which have a strong nonlinear affect on entrainment. When suspended sediment is transported over a partially covered bed of coarse and immobile grains, entrainment also depends on the volume and configuration of fine sediment on the bed. Results from the experiments presented in this paper suggest that for beds partially covered with mobile sediment, entrainment is also a quasi-linear function of sand cover. However, we also found that conditions of partial sand cover were difficult to achieve and could be produced only within a limited rage of discharge and sediment feed combinations. By itself, this result suggests that entrainment rates increase as sand bed elevations drop below the elevation of the exposed immobile grains – sand is rapidly evacuated once the immobile grains are exposed. We observed that the entrainment rate per unit bed area that was covered by sand was higher than would be predicted for a bed completely covered by sand, while the net entrainment rate from the entire bed was lower than expected for a full sand bed. Our results provide a somewhat different perspective on the observations of *Sambrook Smith and Nicholas* [2005], who argue that the transition from gravel to sand beds is a threshold phenomena related to reduced mobility of gravel relative to sand. While our observation of the rapid transition from a bare to sand covered bed also indicates a threshold, our results highlight that this transition may be related entirely to the mobility of the sand fraction, which we suggest is itself a function of the relative sand elevation.

[50] The comparisons made between observed concentrations for conditions of partial sand cover and expected concentrations for a full sand bed and the proposed form for the sand elevation correction rely on our assumption that the Garcia and Parker entrainment function correctly and precisely predicts entrainment for a sand-covered bed. It is important to recognize that such precision rarely exists and observed concentrations frequently deviate from predicted values by an order of magnitude or more [*Garcia and Parker*, 1991]. The sand elevation correction developed in this paper is therefore subject to the same uncertainty. However, the constraints imposed at the extremes of the function and our observations on the bed behavior in the range of partial sand cover conditions support the form of the proposed function.

[51] The sand elevation correction function meets the constraints of diminishing entrainment as the sand bed elevation approaches zero and normal sand bed entrainment as the bed approaches full sand coverage. The correction function also encompasses the competing effects of decreasing sand cover and increasing rate of entrainment per unit sand area. Accelerated local entrainment that occurs as the coarse grains become exposed and generate near-bed turbulence is compensated by the decreasing area of sand that is exposed and available for entrainment. For average sand bed elevations greater than about 0.5 r_b, the effect of enhanced entrainment per unit sand area maintains the net entrainment rate at approximately the rate that occurs for a full sand bed. This results in rapid evacuation of sand once the immobile grains are exposed. When the sand bed elevation decreases below 0.5 r_b, the decreasing area (and volume) of sand available for entrainment begins to restrict the net rate of entrainment, despite high entrainment per unit area that is covered by sand. This decrease in the net entrainment rate can then slow the rate of sand evacuation when the sand bed elevation is less than 0.5 r_b.

[52] Because the data for the range of sand bed elevations between 0.4 r_b and 1.0 r_b are few, our findings do not preclude the possibility that partial sand bed entrainment

rates actually exceed the full sand bed rate for some range of sand bed elevations, as suggested by *Nickling and McKenna Neuman* [1995]. Other factors, such as the narrowness of the experimental channel may also have affected the entrainment conditions. Nevertheless, the proposed sand elevation correction provides some initial guidance on the variation of sand entrainment over a coarse bed for conditions of partial sand cover.

[53] Application of the proposed sand elevation correction requires a determination of the size of the immobile grains and the average height of mobile sediment among those grains, in addition to other parameters that are required for any estimate of suspended sediment transport. The appropriate measure of the immobile grain size is the average difference in elevation between the low points in the interstitial storage spaces and the tops of the immobile grains. For a bed of regular hemispheres, this value is one half the immobile grain diameter. That may be considered comparable to one half the D_{90} in a bed of natural grains, although the suitability of this approximation would depend on the shape of the grains and the degree of sorting in the sediment mixture. The average height of the mobile sediment must be measured directly or estimated from some measure of the spatial extent of sand cover. Sensitivity of entrainment predictions to estimation of the immobile grains size and mobile sediment thickness requires further evaluation.

Notation

A constant = 1.3×10^{-7} in *Garcia and Parker* [1991] entrainment relation.
A_s proportion of bed covered by sand.
a reference elevation for suspended sediment concentration.
b channel width.
c instantaneous concentration of suspended sediment.
c' instantaneous deviation from time average concentration of suspended sediment.
c'_a instantaneous deviation from time average concentration of suspended sediment near the bed.
$\bar{c}$ time average concentration of suspended sediment.
$\bar{c}_a$ time average concentration of suspended sediment near the bed.
$\bar{c}_{a,obs}$ observed near-bed concentration of suspended sediment.
$\hat{c}_a$ observed near-bed concentration normalized by the proportion of bed covered by sand.
D_{50} median size of the mobile sediment.
D_f median fall diameter.
E_s dimensionless rate of entrainment of sand from the bed;.
$\hat{E}_s$ predicted rate of entrainment for a sand-covered bed.
Fr Froude number.
F_z instantaneous upward flux of sediment.
$\bar{F}_z$ time average upward flux of sediment.
$\bar{F}_{za}$ time average upward flux of sediment near the bed.
g gravitational acceleration.
h flow depth.
h_{sk} flow depth due to grain stress, in stress decomposition.
k von Karman's constant = 0.4.
k_s Nikuradse equivalent grain roughness associated with the total bed stress.
$k_{s,sk}$ skin friction roughness height.
L length of bed in streamwise direction.
N number of hemispheres per meter of channel length.
n constant = 0.6 in *Garcia and Parker* [1991] entrainment relation.
P wetted perimeter.
Q discharge.
Q_s sediment discharge.
R hydraulic radius.
Re Reynolds number.
R_p particle Reynolds number for mobile sediment.
R_o Rouse number.
r_b height of immobile coarse grains.
S energy gradient.
S_0 bed slope.
s specific gravity of sediment.
U mean velocity.
u instantaneous streamwise velocity.
u' instantaneous deviation from time average streamwise fluid velocity.
$\bar{u}$ time average streamwise fluid velocity.
u_* shear velocity near the bed.
u_{*sk} skin friction shear velocity near the bed.
$u_*(z)$ shear velocity at height z above the bed.
W vertical velocity of sediment.
w instantaneous vertical fluid velocity.
w' instantaneous deviation from time average vertical fluid velocity.
$\bar{w}$ time average vertical fluid velocity.
w_s particle settling velocity.
Z_m similarity variable in *Garcia and Parker* [1991] entrainment relation.
Z^* parameter in sand elevation correction function.
z elevation above bed.
z_s elevation of sand among immobile coarse grains.
$\bar{z}_s$ spatially averaged sand bed elevation.
$\hat{z}_s$ average sand bed elevation normalized by the height of the immobile grains.
ε proposed sand elevation correction.
ε_A sand elevation correction that would result from entrainment directly proportional to the area of bed covered by sand.
η power in sand elevation correction function.
ν kinematic viscosity.
τ_0 boundary shear stress.
$\tau_{0,SW}$ boundary shear stress calculated using the shallow water equation.
$\tau_{0,RS}$ boundary shear stress calculated from the measured Reynolds stress.
$\tau_{b,RS}$ bed stress based on measured Reynolds stress.
$\tau_{w,RS}$ wall stress based on measured Reynolds stress.
$\tau_{zx}(z)$ turbulent Reynolds stress at height z above the bed.
ξ power in sand elevation correction function.

[54] **Acknowledgments.** Financial support for this work was provided by the Grand Canyon Monitoring and Research Center of the U.S. Geological Survey. Additional support for the laboratory experiments was provided by the St. Anthony Falls Laboratory of the University of Minnesota and the STC program of the National Science Foundation via the National Center for Earth-surface Dynamics under agreement EAR-0120914. Final manuscript preparation was completed while the first author was a postdoctoral research associate under support from the USDA Forest

Service Stream Systems Technology Center. Careful reviews provided by John Pitlick, Mark Schmeeckle, M. Gordon Wolman, and one anonymous reviewer resulted in significant improvements to the presentation of this manuscript.

References

Byrd, T. C., D. J. Furbish, and J. Warburton (2000), Estimating depth-averaged velocities in rough channels, *Earth Surf. Processes Landforms*, *25*(2), 167–173.

Celik, I., and W. Rodi (1988), Modeling suspended sediment transport in nonequilibrium situations, *J. Hydraul. Eng.*, *114*(10), 1157–1191.

Chiew, Y., and G. Parker (1994), Incipient sediment motion on non-horizontal slopes, *J. Hydraul. Res.*, *32*(5), 649–660.

Einstein, H. A., and N. L. Barbarossa (1952), River channel roughness, *Trans. Am. Soc. Civ. Eng.*, *117*, 1121–1146.

Einstein, H. A. and N. Chien (1953), Transport of sediment mixtures with large ranges of grain sizes, *MRD Sediment Ser. 2*, 73 pp., Inst. of Eng. Res., Univ. of Calif., Berkeley.

Engelund, F., and J. Fredsoe (1976), A sediment transport model for straight alluvial channels, *Nord. Hydrol.*, *7*, 293–306.

Engelund, F. and E. Hansen (1967), *A Monograph on Sediment Transport in Alluvial Streams*, Teknisk Forlag, Copenhagen.

Garcia, M., and G. Parker (1991), Entrainment of bed sediment into suspension, *J. Hydraul. Eng.*, *117*(4), 414–435.

Goring, D. G., and V. I. Nikora (2002), Despiking acoustic doppler velocimeter data, *J. Hydraul. Eng.*, *128*(1), 117–126.

Grams, P. E. (2006), Sand transport over a coarse and immobile bed, Ph.D. dissertation, 193 pp., Johns Hopkins Univ., Baltimore, Md.

Itakura, T., and T. Kishi (1980), Open channel flow with suspended sediments, *J. Hydraul. Div. Am. Soc. Civ. Eng.*, *106*(HY8), 1325–1343.

Lisle, T. E., and J. Lewis (1992), Effects of sediment transport on survival of salmonid embryos in a natural stream: A simulation approach, *Can. J. Fish. Aquat. Sci.*, *49*, 2337–2344.

McLean, S. R., S. R. Wolfe, and J. M. Nelson (1999), Predicting boundary shear stress and sediment transport over bed forms, *J. Hydraul. Div. Am. Soc. Civ. Eng.*, *125*(7), 725–736.

Meade, R. H., T. R. Yuzyk, and T. J. Day (1990), Movement and storage of sediment in rivers of the United States and Canada, in *Surface Water Hydrology*, edited by M. G. Wolman and H. C. Riggs, pp. 255–280, Geol. Soc. of Am., Boulder, Colo.

Middleton, G. V. and J. B. Southard (1984), *Mechanics of Sediment Movement, Lecture Notes Short Course*, vol. 3, 401 pp., Soc. of Econ. Paleontol. and Mineral., Tulsa, Okla.

Nelson, J. M., R. L. Shreve, S. R. McLean, and T. G. Drake (1995), Role of near-bed turbulence structure in bed load transport and bed form mechanics, *Water Resour. Res.*, *31*(8), 2071–2086.

Nickling, W. G., and C. McKenna Neuman (1995), Development of deflation lag surfaces, *Sedimentology*, *42*, 403–414.

Nowell, A. R. M., and M. Church (1979), Turbulent flow in a depth-limited boundary layer, *J. Geophys. Res.*, *84*(C8), 4816–4824.

Parker, G., and A. G. Anderson (1977), Basic principles of river hydraulics, *J. Hydraul. Div. Am. Soc. Civ. Eng.*, *103*(HY9), 1077–1087.

Rouse, H. (1937), Modern conceptions of the mechanics of fluid turbulence, *Proc. Am. Soc. Civ. Eng.*, *102*, 463–543.

Sambrook Smith, G. H., and A. P. Nicholas (2005), Effect on flow structure of sand deposition on a gravel bed: Results from a two-dimensional flume experiment, *Water Resour. Res.*, *41*, W10405, doi:10.1029/2004WR003817.

Smith, D. J., and S. R. McLean (1977), Spatially averaged flow over a wavy surface, *J. Geophys. Res.*, *82*(12), 1735–1746.

Trimble, S. W. (1997), Contribution of stream channel erosion to sediment yield from an urbanizing watershed, *Science*, *278*(5342), 1442–1444.

Vanoni, V. A. (1975), *Sedimentation Engineering*, Am. Soc. of Civ. Eng., Reston, Va.

van Rijn, L. C. (1984), Sediment transport, part II: Suspended load transport, *J. Hydraul. Eng.*, *110*(11), 1613–1641.

Wahl, T. L. (2000), Analyzing ADV data using WinADV, paper presented at Joint Conference on Water Resources Engineering and Water Resources Planning and Management, Am. Soc. of Civ. Eng., Minneapolis, Minn.

Wahl, T. L. (2003), Discussion of "Despiking acoustic doppler velocimeter data", *J. Hydraul. Eng.*, *129*(6), 484–487.

Wiberg, P. L., and J. D. Smith (1991), Velocity distribution and bed roughness in high-gradient streams, *Water Resour. Res.*, *27*(5), 825–838.

Willgoose, G., R. L. Bras, and I. Rodriguez-Iturbe (1990), A model of river basin evolution, *Eos Trans. AGU*, *71*(47), 1806.

Wright, S., and G. Parker (2004), Flow resistance and suspended load in sand-bed rivers: Simplified stratification model, *J. Hydraul. Eng.*, *130*(8), 796–805.

P. E. Grams, Department of Watershed Sciences, Utah State University, Logan, UT 84322-5210, USA. (grams@cc.usu.edu)

P. R. Wilcock, Department of Geography and Environmental Engineering, Johns Hopkins University, Baltimore, MD 21218, USA.